Neurodegenerative Diseases

Neurodegener Dis , DOI: 10.1159/000547261
Received: January 20, 2025
Accepted: June 19, 2025
Published online: July 10, 2025

A radiomics-based analysis of functional dopaminergic scintigraphic imaging for the diagnosis of dementia with Lewy bodies

Perriraz J, Abler D, Salvioni Chiabotti P, Hall C, Lejay N, Kurian GK, Vetterli T, Rouaud O, Nicod Lalonde M, Schaefer N, Allali G, Depeursinge A, Prior JO, Jreige M

ISSN: 1660-2854 (Print), eISSN: 1660-2862 (Online)
https://www.karger.com/NDD
Neurodegenerative Diseases

Title: A radiomics-based analysis of functional dopaminergic scintigraphic imaging for the diagnosis of dementia with Lewy bodies

Authors: Jérémy Perriraz[1], Daniel Abler[3,4,5], Paolo Salvioni Chiabotti[2], Caroline Hall[2], Noemie Lejay[2], George K. Kurian[1], Thomas Vetterli[1], Olivier Rouaud[2], Marie Nicod Lalonde[1], Niklaus Schaefer[1], Gilles Allali[2], Adrien Depeursinge[1,5,6], John O. Prior[1], Mario Jreige[1]

Affiliation:
[1] Department of Nuclear Medicine and Molecular Imaging, Lausanne University Hospital, Lausanne, Switzerland.
[2] Leenaards Memory Center, Department of Clinical Neurosciences, Lausanne University Hospital and University of Lausanne, Lausanne, Switzerland.
[3] Department of Oncology, Lausanne University Hospital, Lausanne, Switzerland.
[4] Department of Oncology, Geneva University Hospitals, Geneva, Switzerland.
[5]Lundin Family Brain Tumour Research Centre, Lausanne University Hospital, Lausanne, Switzerland.
[6] Institute of Informatics, HES-SO Valais-Wallis University of Applied Sciences and Arts Western Switzerland, Sierre, Switzerland.

Corresponding author
Professor John O. Prior
Department of Nuclear Medicine and Molecular Imaging
Lausanne University Hospital, Rue du Bugnon 46, CH-1011 Lausanne, Switzerland
E-mail: john.prior@chuv.ch

Keywords: Dopaminergic Imaging; DaTscan; 123-FP-CIT; SPET/CT; Dementia with Lewy bodies; DLB; Radiomics

Running title: Radiomics for Dopaminergic Imaging in DLB Diagnosis

Word count: 2814

Abstract

Introduction
Radiomics features, a technique based on quantitative image analysis, can be used to capture tissue and lesion characteristics, such as heterogeneity and shape. Using functional dopaminergic scintigraphy, we aim to study the value of radiomics features in predicting the diagnosis of dementia with Lewy bodies (DLB).

Materials and methods
We retrospectively analyzed 74 patients (29 F and 45 M, mean age 71.6±9.2) investigated in the Leenaards Memory Center (Lausanne University Hospital) for DLB who underwent quantitative I-123-ioflupane SPECT/CT (DaTscan). All scanned examinations had xSPECT reconstruction, allowing SUV quantification. We segmented the right and left striatum using 3D Slicer and performed radiomics feature extraction and analysis using the QuantImage v2 platform. The dataset was divided into training (80%) and test (20%) sets, and various classification algorithms were used to predict the definitive clinical diagnosis of DLB using xSPECT and/or clinical features. Receiver operating characteristic (ROC) curve analysis was performed to characterize the performance of the obtained models.

Results
Thirty-three of 74 patients (45%) were diagnosed with DLB. The xSPECT radiomics models showing the highest diagnostic performance were developed based on nine non-correlated features from both striatal regions and a support vector classifier (SVC) algorithm. The xSPECT radiomics models demonstrated superior performance

compared to models based on SUV intensity features alone (p=0.001) or clinical features alone (p=0.001), with AUC values of 0.932 (0.920–0.944), 0.856 (0.840–0.875), and 0.793 (0.770–0.815), respectively. The combined model, incorporating both clinical and xSPECT features, achieved the highest overall performance with a sensitivity of 100% (95% CI: 100–100), specificity of 89.7% (87.6–91.4), and an AUC of 0.956 (0.945–0.964).

Conclusion
The radiomics model based on quantitative I-123-ioflupane xSPECT/CT showed high diagnostic accuracy in predicting the diagnosis of DLB using diverse features derived from striatal analysis. This tool may improve the diagnostic accuracy of I-123-ioflupane, which is of major importance for DLB diagnosis.

Introduction

Lewy body dementia (DLB) is the second most common form of neurodegenerative dementia after Alzheimer Disease (AD), accounting for 15–25% of all dementia cases [1]. Neuropathological findings in patients with DLB include neuronal degeneration in the neocortex, limbic system, and brainstem as well as Lewy bodies and Lewy neurites positive for α-synuclein immunohistochemical staining [2]. DLB is clinically diagnosed by identifying key clinical features: fluctuations, visual hallucinations, rapid eye movement (REM) sleep, and parkinsonism. The fourth and most recent consensus for the diagnosis of DLB includes reduced dopamine transporter uptake in the basal ganglia, as shown by single positron emission computed tomography (SPECT) as an indicative biomarker [3].

From a clinical point of view, distinguishing DLB from other forms of dementia is of utmost clinical importance, as the subsequent clinical and therapeutic management of patients is different, especially to avoid improper use of antipsychotic drugs in DLB patients [4]. As life expectancy is shorter in DLB, the course of the disease is also different. However, distinguishing DLB from other forms of dementia can be difficult, particularly in the elderly, who are often affected by combined neurodegenerative and cerebrovascular conditions.

Radiomics is an evolving research field that aims to capture detailed tissue and lesion characteristics by using quantitative medical image analysis. Radiomics features, characterizing for example the shape, intensity distribution and texture of regions-of-interest (ROI) are valuable for clinical problem-solving. With sufficiently large datasets, radiomics data can reveal previously unknown markers and patterns related to disease development, progression, and treatment response [5][6]. This suggests that the application of radiomics analysis techniques to functional dopaminergic scintigraphy imaging could reveal novel biomarkers for diagnosing DLB.

This study aimed to investigate the potential of radiomics-based analysis of functional dopaminergic scintigraphy imaging for predicting the diagnosis of DLB.

Materials and methods

Study design and patient selection

This was a retrospective, single-center study. Patients were selected from a cohort at the Leenaards Memory Center (Lausanne University Hospital). All patients were followed up for at least 2 years after DaTscan, and the final diagnosis was confirmed by two behavioral neurologists (PSC and CH).
The inclusion criteria were as follows: (a) patients who were followed up for diagnostic workup and underwent dopaminergic scintigraphic imaging (DaTscan for dopaminergic assessment with quantitative SPECT/CT acquisition), and (b) patients investigated for DLB with a definitive diagnosis validated by the neurology team.
The exclusion criteria were as follows: (a) patients aged < 18 years and (b) patients without quantitative SPECT/CT acquisition.
The local Ethics Research Committee of the State of Vaud approved the research protocol (CER-VD #2018-01513). All patients participating in this study had signed an institutional general informed consent form for the retrospective use of their data in clinical research.

Reference standard

The reference standard for diagnosing DLB follows the criteria outlined in the fourth consensus report of the DLB Consortium [3]. This diagnosis is clinically based on the essential, core, and supportive features. The essential feature is the presence of dementia, while the core clinical features include fluctuating cognition, recurrent visual hallucinations, REM sleep behavior disorder (RBD), and parkinsonism. Indicative or supportive biomarkers such as reduced dopamine transporter uptake in the basal ganglia, as shown by SPECT or PET imaging, can provide additional diagnostic support. These may contribute to the diagnosis of DLB when combined with essential and/or core clinical features.

Image acquisition

All patients underwent quantitative xSPECT/CT (Siemens Symbia Intevo, Erlangen, Germany), centered on the striatal regions of the brain. The xSPECT images were acquired on average at 4h42 ± 44 min after intravenous injection of 179 ± 17 MBq of I-123-ioflupane. Images were acquired with a 3 °rotation/step and 30 s/projection

using a 256 × 256 matrix. Reduced-dose CT was performed using 120 kV and 25 reference mAs modulation (Siemens Care Dose; Symbia Intevo, Erlangen, Germany). Images were reconstructed using conventional iterative reconstruction (FLASH 3D) and quantitative xSPECT reconstruction. The xSPECT reconstruction algorithm allows SUVbw quantification on post-processed images and measurement of the standard uptake value (SUV).

Striatum segmentation

The images were anonymized and exported to 3D Slicer. Segmentation of the left and right striata was performed using a threshold-based semi-automated method (set at 40% of SUVmax), followed by a consensus review by two physicians on both SPECT and fusion SPECT/CT images. This consensus approach aimed to minimize variability, although formal inter-rater reliability metrics were not computed.

Clinical variables

The presence or absence of the following clinical variables used in the diagnosis of DLB was retrieved from the electronic medical records for each patient: visual hallucinations, REM sleep behavior disorder (RBD), cognitive fluctuations, and parkinsonism.

Radiomics feature extraction and predictive modelling

Coded patient images and striatum segmentations were uploaded to the QuantImage v2 (QI) platform for radiomics analysis and predictive modeling [7]. A total of 212 radiomics features, capturing the shape, intensity distribution, and texture, were extracted from both striatal areas separately in xSPECT using built-in pyradiomics and Riesz feature extractors, resulting in 424 radiomics features per patient [8][9].

We developed four distinct models for predicting DLB diagnosis: two based solely on features derived from xSPECT, one using only clinical features, and one combining imaging and clinical data. The dataset was divided into training (80%) and test (20%) sets, with feature values standardized according to individual means and standard deviations from the training set. A Spearman correlation matrix was computed, and features with $r > 0.8$ were excluded prior to selection. For each model, the most relevant features from both striata were selected in two steps: first, by removing redundant features (Spearman correlation > 0.8), and then by choosing the 20 features with the highest univariate predictive scores for DLB according to the ANOVA F-score, computed on the training set (Figure 1).

The most predictive xSPECT models for this classification task were determined using a grid search with 5-fold stratified cross-validation on the training set. The generalization performance of the model was evaluated on the test set using the area under the ROC curve (AUC) as a performance metric. All models were built using the Scikit-learn library integrated into QuantImage v2 [10]. Feature importance was assessed in terms of permutation feature importance, which measures how much a given model relies on a particular feature by breaking the relationship between the feature and the target [11].

Statistical analysis

Continuous variables were reported as mean ± standard deviation (SD). Continuous variables are presented as mean ± standard deviation (SD) along with their range. Categorical data were analyzed using either Fisher's exact test or chi-squared test, depending on the appropriateness of the data. The Student's t-test was used for comparisons between the two groups.

Confidence intervals (CIs) for the average model performance were determined through bootstrapping (n=20) from a collection of k performance estimates, producing n sets of k performance estimates. The mean performance estimates were calculated for each set. The 95% CI was defined as the interval between the 2.5th and 97.5th percentiles of the bootstrap distribution of mean performance estimates. For cross-validation performance, bootstrapping was applied to the k=5 performance estimates from 5-fold cross-validation. For the test performance, the k performance estimates needed for CI computation were obtained by evaluating the prediction model on 100 bootstrapped samples of the test dataset.

Differences in model performance were evaluated using pairwise permutation tests between the k-test performance estimates of the two models with a significance threshold of $p<0.05$.

Results

Patient population

A total of 108 patients from the Leenaards Memory Center were investigated for dementia with DLB. Of these, 34 patients were excluded because of the absence of analyzable quantitative SPECT/CT acquisitions. The remaining 74 patients who underwent DAT scan with quantitative acquisition were categorized as having either a definitive diagnosis of DLB or a diagnosis of non-DLB (Figure 2). The final study population included 74 patients (mean age 71.6±9.2 years, 40 % female (n=45/74)). Table 1 summarizes patient demographics and clinical features.

Model comparison

Model metrics, including model type, number of features used, AUC, accuracy, precision, sensitivity, and specificity for the two models derived from xSPECT alone, the model derived from clinical features alone and the combined clinical and xSPECT model, are reported in Table 2.

The first xSPECT model was constructed using texture, SUV intensity, and shape features, whereas the second model relied solely on SUV intensity features. The clinical model showed sensitivity, specificity, and AUC of 40.6% (37.8–44), 87.3% (85.4–89), and 0.793 (0.770–0.815), respectively. The SUV model showed better performance in distinguishing DLB from non-DLB (p=0.005), with a sensitivity, specificity, and AUC of 71.3% (68.7–74.3), 78.7% (75.9–80.4), and 0.856 (0.840–0.875), respectively. The performance of the xSPECT model using nine features was higher than that of the clinical (p=0.001) and SUV (p=0.001) models, with a sensitivity, specificity, and AUC of 100% (100–100), 87.9% (85.5–89.9), and 0.932 (0.920–0.944), respectively. The combined clinical and xSPECT model was based on 13 features and exhibited significantly better diagnostic performance than the xSPECT (p=0.007), SUV (p=0.001), and clinical (p=0.001) models with a sensitivity of 100% (95% CI: 100–100), specificity of 89.7% (87.6–91.4), and an AUC of 0.956 (0.945–0.964), respectively. All the four models were developed using a support vector classifier algorithm. The most predictive features included a combination of texture features (e.g., GLCM_Correlation and GLDM_LargeDependenceEmphasis), shape features (e.g., sphericity), and intensity-based measures (e.g., SUVmax and SUVmean). Texture features such as GLCM_Correlation may reflect striatal heterogeneity associated with dopaminergic denervation, whereas shape-based metrics could be related to striatal atrophy or asymmetry. These features, derived from both the left and right striata, had the highest permutation importance in the xSPECT and combined models (Figure 3). The performance metrics for the training set, computed using 5-fold cross-validation, are provided in Supplementary Table 1.

Discussion

In this study, we examined radiomics analysis models based on quantitative I-123-ioflupane SPECT/CT. Our models incorporated various radiomics features extracted from xSPECT images, including texture, SUV, and shape characteristics. We also evaluated a benchmark model using only the clinical features of DLB and compared it with an imaging model that integrated the most relevant xSPECT radiomics features. The xSPECT model based on striatal I-123-ioflupane uptake quantification using texture, SUV, and shape features outperformed those relying solely on the SUV or clinical features. The highest predictive performance for DLB was achieved by combining the imaging features with clinical data. While the combined model achieved a sensitivity of 100% on the independent test set, we recognize that although promising, such a result comes at the cost of imperfect specificity and may reflect potential overfitting due to the limited sample size and the absence of external validation. The test set was separated from the training set before the feature selection and model development to ensure independence. Nevertheless, this finding highlights the need for validation in larger and independent multicenter cohorts to confirm the generalizability and robustness of the proposed model.

Radiomics holds significant promise as a biomarker for distinguishing Lewy body dementia (DLB) from other forms of dementia, and can improve the diagnosis, prognosis, and management of dementia. Our results underscore the potential of radiomics as a biomarker for differentiating Lewy body dementia (DLB) from other forms of dementia. Numerous studies have shown the potential for the clinical application of radiomics features in nuclear medicine studies, mainly in oncologic imaging. For instance, radiomics features have been shown to allow prediction of diagnosis, prognosis, risk of recurrence, and differential diagnosis, leading to better predictions of overall survival and more appropriate treatment choices, thereby improving patient management [12][13][14]. Similar advancements have been observed in dementia research, including studies of Parkinson's disease (PD), Alzheimer's disease (AD), amnestic mild cognitive impairment (aMCI/MCI), frontotemporal dementia (FTD), and DLB [15][16][17][18][19][20][21]. These studies extracted radiomics features from MRI or 18-F-FDG PET/CT and evaluated models based on imaging radiomics features alone, as well as those combining clinical and imaging data.

All approaches demonstrated promising results in terms of enhancing diagnostic accuracy. Similarly, our models applied to DLB align with these findings, showing strong performance in diagnosing DLB and indicating a potential advancement in the diagnostic process for this complex condition, particularly when combining xSPECT and clinical features.
The radiomics models used in this study were based on I-123-ioflupane SPECT imaging (DaTscan) using xSPECT reconstruction for SUV quantification. This imaging and reconstruction method has been widely used in both quantitative and semiquantitative analyses. Comparing our results with similar techniques is crucial because I-123-ioflupane SPECT is an established biomarker for diagnosing DLB [3].

Quantitative and semiquantitative approaches using I-123-ioflupane SPECT imaging, such as DaTscan, have consistently demonstrated superior diagnostic accuracy in distinguishing neurodegenerative dementias, including DLB, AD, and PD. Several studies have employed I-123-ioflupane SPECT and semi-quantitative techniques such as caudate binding potential (CBP), putamen binding potential (PBP), and putamen/caudate ratio (PCR), demonstrating superior results over visual and qualitative diagnosis in differentiating dementia such as AD, DLB, and FTD [22][23][24]. Additionally, the combination of semi-quantitative indicators with radiomics features has been suggested to improve the classification accuracy of Parkinson's disease compared to healthy controls [25]. For quantitative techniques, studies have used DaTscan alongside methods such as BRASS, QuantiSPECT, and/or DaTQUANT, which have proven effective in reducing equivocal reports and distinguishing between Parkinson's and essential tremor [26] [27]. Furthermore, quantitative metrics such as SUV_max, SUV_mean, and SUR_relative quantification have shown promise in differentiating DLB from PD and control cases [28]. A notable study compared three quantitative methods (MIMneuro, DaTQUANT, and manual) for detecting DLB, reporting AUCs comparable to ours, ranging from over 0.930 to 1.000 ($P < 0.001$) and excellent discrimination between DLB and non-DLB cases [29]. These findings underscore the potential of DaTscan quantification in the diagnosis of neurodegenerative dementia. While our radiomics-based approach demonstrated comparable or superior diagnostic accuracy to previously published methods, we did not apply commercially available semi-quantitative tools, such as DaTQUANT or BRASS, in our cohort. Therefore, a direct head-to-head comparison with these reference methods was not feasible. Nevertheless, previously published studies using DaTQUANT or MIMneuro have reported AUCs ranging from 0.930 to 1.000 for differentiating DLB from other neurodegenerative disorders, which are broadly consistent with the performance of our combined model. Future studies should include a direct comparison of radiomics-based methods with standardized commercial quantification tools to confirm their added value in clinical settings.

Recent advancements in radiomics and deep learning have highlighted the potential of integrating imaging and clinical features for improved diagnostic accuracy, which further underscores the feasibility of using xSPECT-derived data to enhance the differentiation of DLB. In a recent study, Jiang et al. explored the use of 123I-Ioflupane SPECT radiomics analysis combined with deep learning (DL) to predict the Hoehn-Yahr stages (HYS) of Parkinson's disease. They found that integrating radiomics and deep learning features improved the prediction accuracy compared to using either approach alone, potentially facilitating earlier diagnosis and treatment of patients with PD. Notably, the study also reported no significant differences in radiomics results between MRI- and SPECT-based striatal segmentations for both radiomics and deep learning features [30]. To our knowledge, this is the first study to explore I-123-Ioflupane SPECT radiomics for diagnosing DLB by integrating imaging and specific clinical features. Our findings demonstrate that radiomics analysis of I-123-ioflupane uptake using xSPECT-derived data is both feasible and promising for distinguishing between normal and pathological I-123-ioflupane uptake associated with DLB. This method has the potential to greatly improve the diagnostic accuracy, sensitivity, and specificity for Lewy body dementia compared to traditional quantitative methods that rely solely on SUV values or clinical features alone. Furthermore, it could pave the way for developing predictive models based on radiomics features, offering the capability to accurately classify patients across the spectrum of DLB.

Our study had several limitations, such as the absence of neuropathological confirmation. Although I-123-Ioflupane SPECT is frequently used as an adjunctive tool for diagnosing Lewy body dementia, it can pose limitations for reference standard definitions. This issue was partially addressed by comparing purely clinical models with imaging-only and combined clinical and imaging models. In addition, although segmentation was performed using a semi-automated approach with consensus review, inter-rater agreement metrics were not formally assessed, which may have affected reproducibility across readers. Furthermore, we segmented the

entire striatum rather than conducting sub-segmentation of the putamen and caudate nucleus, which could have provided more precise insights into disease pathophysiology. Another limitation is the heterogeneity of the non-DLB group, which included a range of neurodegenerative and non-neurodegenerative conditions such as Alzheimer's disease, frontotemporal dementia, vascular dementia, and Parkinson's disease. While this reflects the diagnostic complexity typically encountered in memory clinics, it may also affect the specificity of the model and should be considered when interpreting the results.

Additionally, several factors may have influenced the generalizability of our findings. The comparison group in our study was heterogeneous, including patients with Alzheimer's disease, frontotemporal dementia, and vascular, parkinsonian, and other etiologies. While this reflects the clinical reality of differential diagnosis in memory clinics, it may also impact the specificity of the model. Moreover, potential confounding effects from medications (e.g., dopaminergic agents, antipsychotics), comorbid neurological or systemic conditions, and image acquisition artifacts were not systematically controlled. As the study was based on data acquired from a single SPECT/CT system at a single institution, variability related to scanner calibration, reconstruction protocols, or patient preparation may limit reproducibility across centers. Finally, the absence of an external validation cohort represents a significant limitation, and underlines the need for multicenter studies to confirm the robustness and applicability of the proposed radiomics model.

To address these limitations, future research should involve multicenter cohorts with pathological diagnosis and external validation to develop algorithms capable of accurately stratifying various types of dementia, including the full spectrum of Lewy body dementia.

Although we did not apply Shapley Additive Explanations (SHAP) analysis in this study owing to the relatively small sample size and computational constraints, we recognize its value for enhancing model transparency. Future work will incorporate SHAP to better quantify and visualize the contribution of individual radiomics features to model predictions. From a clinical perspective, the proposed radiomics-based tool could serve as a decision support system for nuclear medicine physicians and behavioral neurologists in tertiary memory centers. It may be particularly valuable in diagnostically uncertain cases or in settings where equivocal visual or semi-quantitative assessments limit diagnostic confidence. Integration into existing post-processing platforms could facilitate more standardized reporting and enhance the interpretability of I-123-ioflupane SPECT/CT results in routine practice.

Conclusion

The radiomics model based on quantitative I-123-ioflupane xSPECT/CT **demonstrated a high diagnostic accuracy** in predicting the definitive clinical diagnosis of DLB by leveraging diverse striatal features. When combined with the clinical features of DLB, this tool has the potential to significantly improve the diagnostic accuracy of I-123-ioflupane, which is critical for DLB diagnosis, particularly given the recent approval of disease-modifying therapies for Alzheimer's disease. However, to validate and enhance the robustness of this model, further research with larger patient cohorts and external validation is required.

Statement of Ethics

The study protocol was reviewed and approved by the local Ethics Research Committee of the State of Vaud (approval number CER-VD #2018-01513). All patients participating in this study had signed an institutional general informed consent form for the retrospective use of their data in clinical research.

Conflict of Interest Statement

Gilles Allali was a member of the journal's Editorial Board at the time of submission. The other authors declare that they have no competing interest.

Funding Sources

Daniel Abler received funding from the Lundin Family Brain Tumour Research Centre at CHUV which also contributed to the development of QuantImage used for radiomics analysis in this study. This study was supported by a joint grant from the Lausanne University Hospital Foundation and the Private Foundation of Geneva University Hospital (Project #ROMENS 22). GA received fundings from the Faculty of Biology and Medicine of the University of Lausanne, the Swiss National Science Foundation (#214855), the Leenaards Foundation, the Solis Foundation, the Empiris Foundation and the Marina Cuennet-Mauvernay Foundation.

Author Contributions

JP, MJ, AD and JOP conceptualized and designed the study. Cohort curation and clinical evaluation was performed PSC, CH, NL, GK, OR, and GA. Radiomics analysis was performed by JP, MJ, DA, TV and AD. Data analysis and interpretation were carried out by MJ, AD and DA. MJ, GA, and JOP provided critical revisions and supervised the study. JP drafted the manuscript with significant input from MJ, DA, AD, NS, MNL and GA. All authors reviewed, edited, and approved the final version of the manuscript.

Data Availability Statement

The data that support the findings of this study are not publicly available due to technical reasons but are available from the corresponding upon reasonable request.

References

1 Geser F, Wenning GK, Poewe W, McKeith I. How to diagnose dementia with Lewy bodies: state of the art. Mov Disord. 2005 Aug;20 Suppl 12:S11-20.

2 Walker Z, Possin KL, Boeve BF, Aarsland D. Lewy body dementias. Lancet. 2015 Oct;386(10004):1683–97.

3 McKeith IG, Boeve BF, Dickson DW, Halliday G, Taylor J-P, Weintraub D, et al. Diagnosis and management of dementia with Lewy bodies: Fourth consensus report of the DLB Consortium. Neurology. 2017 Jul;89(1):88–100.

4 Taylor J-P, McKeith IG, Burn DJ, Boeve BF, Weintraub D, Bamford C, et al. New evidence on the management of Lewy body dementia. Lancet Neurol. 2020 Feb;19(2):157–69.

5 Rahmim A, Huang P, Shenkov N, Fotouhi S, Davoodi-Bojd E, Lu L, et al. Improved prediction of outcome in Parkinson's disease using radiomics analysis of longitudinal DAT SPECT images. NeuroImage: Clinical. 2017 Jan;16:539–44.

6 Mayerhoefer ME, Materka A, Langs G, Häggström I, Szczypiński P, Gibbs P, et al. Introduction to Radiomics. Journal of Nuclear Medicine. 2020 Apr;61(4):488–95.

7 Abler D, Schaer R, Oreiller V, Verma H, Reichenbach J, Aidonopoulos O, et al. QuantImage v2: a comprehensive and integrated physician-centered cloud platform for radiomics and machine learning research. European Radiology Experimental. 2023 Mar;7(1):16.

8 van Griethuysen JJM, Fedorov A, Parmar C, Hosny A, Aucoin N, Narayan V, et al. Computational Radiomics System to Decode the Radiographic Phenotype. Cancer Research. 2017 Oct;77(21):e104–7.

9 Dicente Cid Y, Muller H, Platon A, Poletti P, Depeursinge A. 3D Solid Texture Classification Using Locally-Oriented Wavelet Transforms. IEEE Trans Image Process. 2017 Apr;26(4):1899–910.

10 Buitinck L, Louppe G, Blondel M, Pedregosa F, Mueller A, Grisel O, et al. API design for machine learning software: experiences from the scikit-learn project. 2013 Sep [cited 2024 Aug 30]. Available from: http://arxiv.org/abs/1309.0238

11 Breiman L. Random Forests. Machine Learning. 2001 Oct;45(1):5–32.
12 Maino C, Vernuccio F, Cannella R, Franco PN, Giannini V, Dezio M, et al. Radiomics and liver: Where we are and where we are headed? European Journal of Radiology. 2024 Feb;171:111297.
13 Gonçalves M, Gsaxner C, Ferreira A, Li J, Puladi B, Kleesiek J, et al. Radiomics in Head and Neck Cancer Outcome Predictions. Diagnostics. 2022 Nov;12(11):2733.
14 Miranda J, Horvat N, Araujo-Filho JAB, Albuquerque KS, Charbel C, Trindade BMC, et al. The Role of Radiomics in Rectal Cancer. J Gastrointest Canc. 2023 Dec;54(4):1158–80.
15 Park CJ, Eom J, Park KS, Park YW, Chung SJ, Kim YJ, et al. An interpretable multiparametric radiomics model of basal ganglia to predict dementia conversion in Parkinson's disease. NPJ Parkinsons Dis. 2023 Aug;9(1):127.
16 Feng Q, Niu J, Wang L, Pang P, Wang M, Liao Z, et al. Comprehensive classification models based on amygdala radiomic features for Alzheimer's disease and mild cognitive impairment. Brain Imaging Behav. 2021 Oct;15(5):2377–86.
17 Zhao K, Ding Y, Han Y, Fan Y, Alexander-Bloch AF, Han T, et al. Independent and reproducible hippocampal radiomic biomarkers for multisite Alzheimer's disease: diagnosis, longitudinal progress and biological basis. Science Bulletin. 2020 Jul;65(13):1103–13.
18 Zhao Y, Zhang J, Chen Y, Jiang J. A Novel Deep Learning Radiomics Model to Discriminate AD, MCI and NC: An Exploratory Study Based on Tau PET Scans from ADNI. Brain Sci. 2022 Aug;12(8):1067.
19 Mattoli MV, Cocciolillo F, Chiacchiaretta P, Dotta F, Trevisi G, Carrarini C, et al. Combined 18F-FDG PET-CT markers in dementia with Lewy bodies. Alzheimer's & Dementia: Diagnosis, Assessment & Disease Monitoring. 2023;15(4):e12515.
20 Ding Y, Zhao K, Che T, Du K, Sun H, Liu S, et al. Quantitative Radiomic Features as New Biomarkers for Alzheimer's Disease: An Amyloid PET Study. Cerebral Cortex. 2021 Aug;31(8):3950–61.
21 Tafuri B, Filardi M, Urso D, De Blasi R, Rizzo G, Nigro S, et al. Radiomics Model for Frontotemporal Dementia Diagnosis Using T1-Weighted MRI. Front Neurosci. 2022;16:828029.
22 Oliveira FPM, Walker Z, Walker RWH, Attems J, Castanheira JC, Silva Â, et al. 123I-FP-CIT SPECT in dementia with Lewy bodies, Parkinson's disease and Alzheimer's disease: a new quantitative analysis of autopsy confirmed cases. J Neurol Neurosurg Psychiatry. 2021 Jun;92(6):662–7.
23 Nicastro N, Garibotto V, Allali G, Assal F, Burkhard PR. Added Value of Combined Semi-Quantitative and Visual [123I]FP-CIT SPECT Analyses for the Diagnosis of Dementia With Lewy Bodies. Clin Nucl Med. 2017 Feb;42(2):e96–102.
24 Spehl TS, Frings L, Hellwig S, Weiller C, Hüll M, Meyer PT, et al. Role of semiquantitative assessment of regional binding potential in 123I-FP-CIT SPECT for the differentiation of frontotemporal dementia, dementia with Lewy bodies, and Alzheimer's dementia. Clin Nucl Med. 2015 Jan;40(1):e27-33.
25 Shiiba T, Takano K, Takaki A, Suwazono S. Dopamine transporter single-photon emission computed tomography-derived radiomics signature for detecting Parkinson's disease. EJNMMI Research. 2022 Jun;12(1):39.
26 Pencharz DR, Hanlon P, Chakravartty R, Navalkissoor S, Quigley A-M, Wagner T, et al. Automated quantification with BRASS reduces equivocal reporting of DaTscan (123I-FP-CIT) SPECT studies. Nucl Med Rev Cent East Eur. 2014;17(2):65–9.
27 Morton RJ, Guy MJ, Clauss R, Hinton PJ, Marshall CA, Clarke EA. Comparison of different methods of DaTscan quantification. Nucl Med Commun. 2005 Dec;26(12):1139–46.
28 Jreige M, Allenbach G, Meyer M, Nicod-Lalonde M, Schaefer N, Benninger D, et al. I-123-ioflupane quantification in Lewy Body Dementia and Parkinson Disease using xSPECT-derived absolute and relative SUV: an updated analysis. Journal of Nuclear Medicine. 2021 May;62(supplement 1):1069–1069.
29 Maltais DD, Jordan LG, Min H-K, Miyagawa T, Przybelski SA, Lesnick TG, et al. Confirmation of 123I-FP-CIT SPECT Quantification Methods in Dementia with Lewy Bodies and Other Neurodegenerative Disorders. J Nucl Med. 2020 Nov;61(11):1628–35.
30 Jiang H, Du Y, Lu Z, Wang B, Zhao Y, Wang R, et al. Radiomics incorporating deep features for predicting Parkinson's disease in 123I-Ioflupane SPECT. EJNMMI Physics. 2024 Jul;11(1):60.

Figure legends

Figure 1. Flowchart illustrating the technical pipeline of the study. Created in BioRender. Prior, J. (2024) BioRender.com/b23m007

Figure 2. Flowchart detailing patient inclusion process.

Figure 3. Feature list and importance for all four models. Permutation-based feature importance for all four models, showing the top-ranked features from both striatal regions. Texture, shape, and intensity-based features are represented. Values > 0 indicate a positive contribution to model performance, as implemented by Scikit-learn [11]. These reflect how the performance of the model is modified when the feature value is randomly shuffled. Values of zero and below indicate features with no positive impact on performance.
Segments 1 and 2 refer to the left and right striata, respectively. PT: single photon emission computerized tomography; MTV: Metabolic Volume; GLCM: Gray-Level Co-Occurrence Matrix; GLDM : Gray Level Dependence Matrix; RBD: Rapid eye movement (REM) sleep behavior disorder.

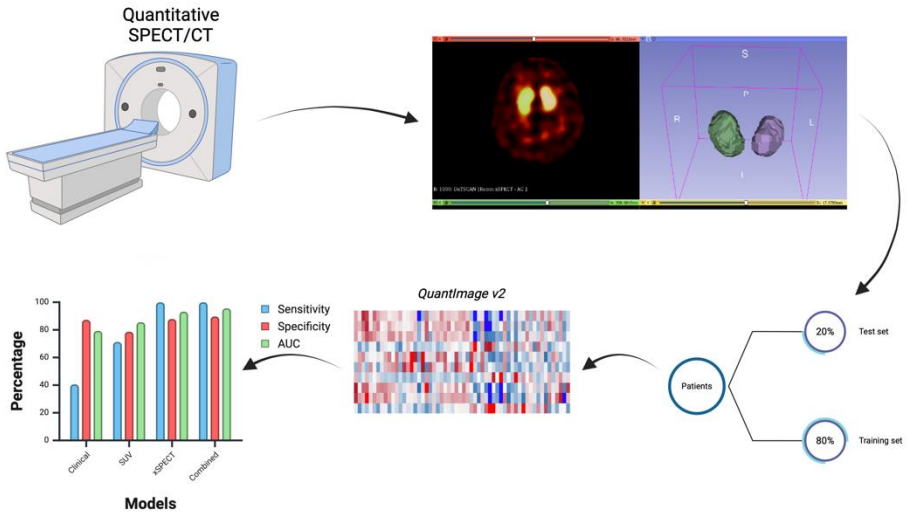

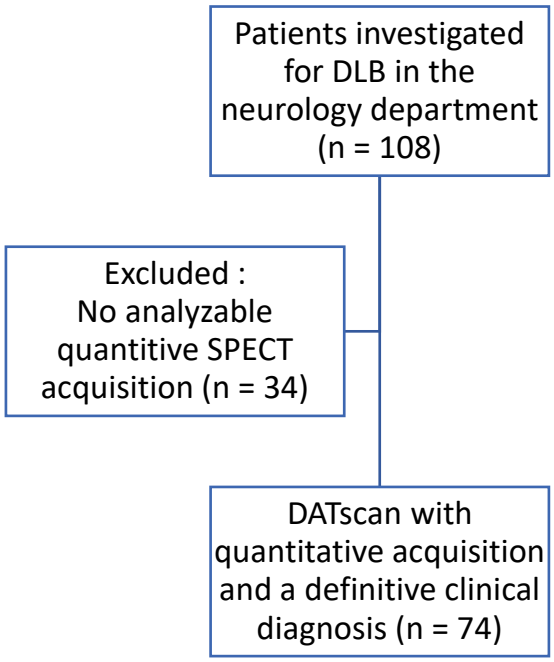

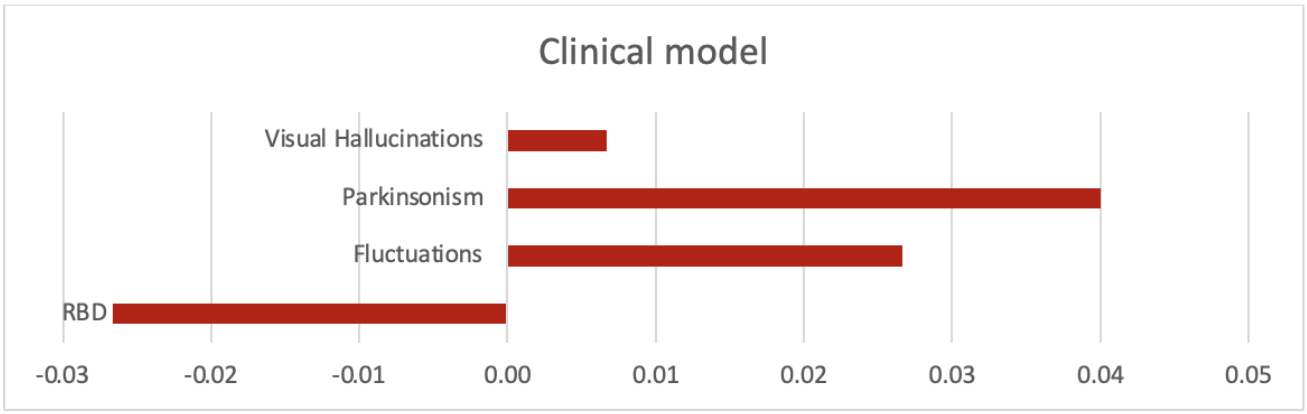

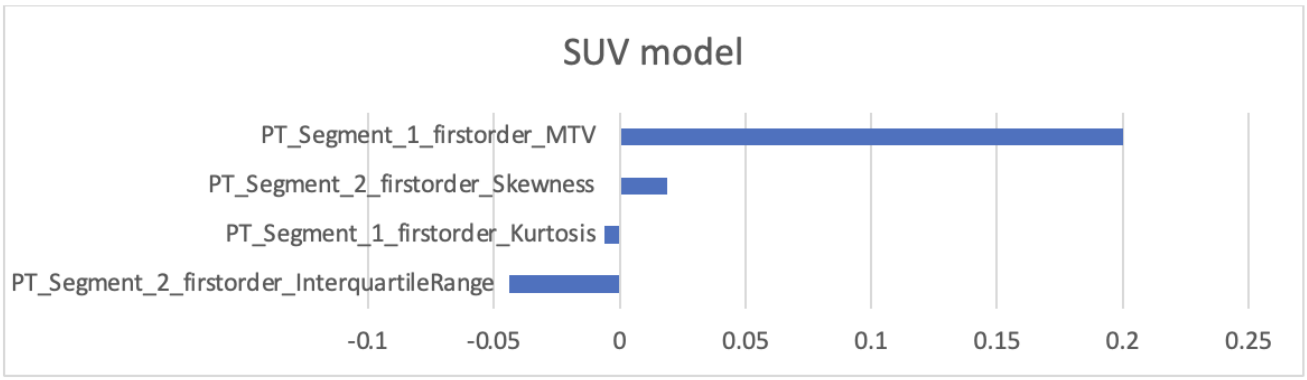

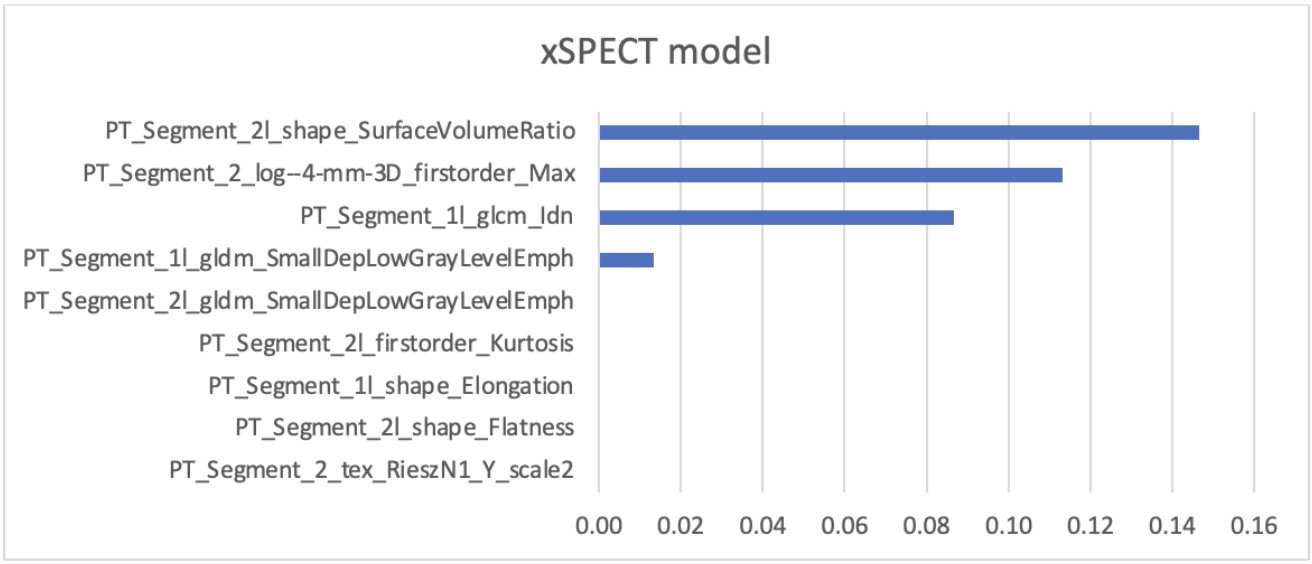

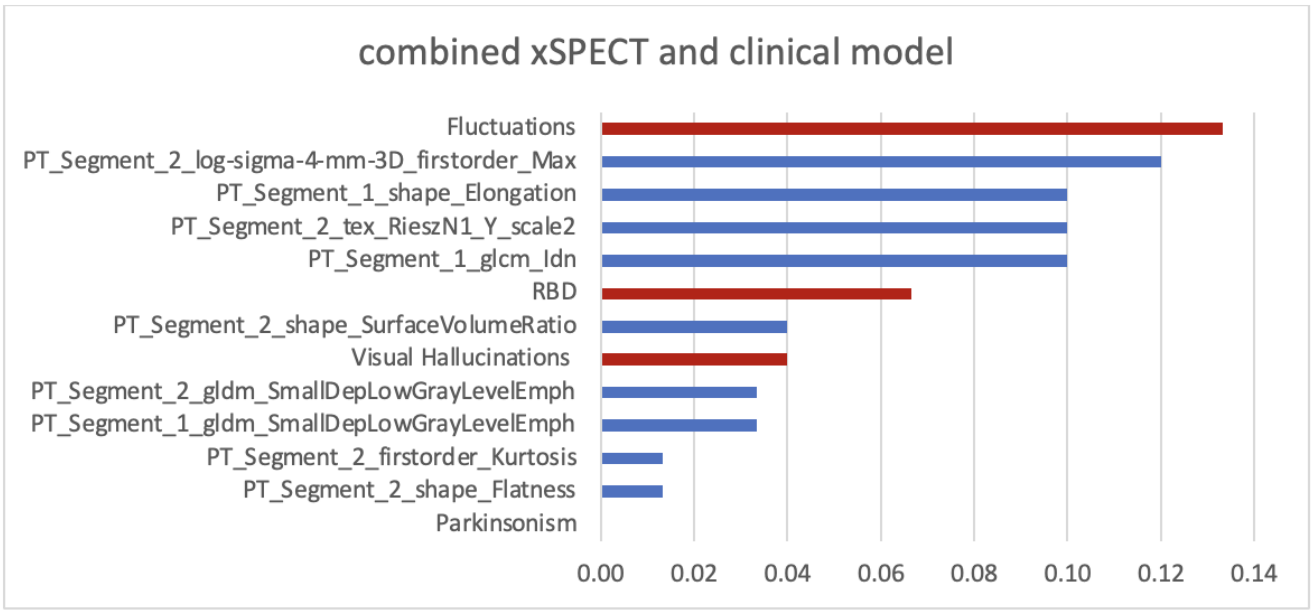

Table 1. Patient population characteristics and clinical features.

Characteristics		DLB	Others*	p-value
	Number of subjects	33/74 (45%)	41/74 (55%)	
	Female/Male	8/25 (24%/76%)	21/20 (51%/49%)	0.018
	Age	71±10	70 ±14	0.774
Symptoms				
	Visual hallucinations	11/33 (33%)	11/41 (27%)	0.543
	RBD	11/33 (33%)	9/41 (22%)	0.273
	Fluctuations	22/33 (67%)	15/41 (37%)	0.010
	Parkinsonism	28/33 (85%)	28/41 (68%)	0.099

*Others: alcohol, alzheimer's disease, corticobasal degeneration, frontotemporal dementia, functional neurological disorders, hypoxic, iatrogenic, idiopathic normal-pressure hydrocephalus, idiopathic Parkinson's disease, multiple system atrophy, neurodevelopmental, not applicable, progressive supranuclear palsy, thymic, vascular.

Legend: dementia with Lewy bodies (DLB), REM sleep behavior disorder (RBD).

Table 2. Model metrics on test datasets for different models tested. The mean and 95% CI were reported for the area under the curve (AUC), accuracy, precision, sensitivity, and specificity. All models were built using the Support Vector Classifier algorithm.

Model	Number of features	AUC	Accuracy	Precision	Sensitivity	Specificity
Clinical model	4	0.793 (0.770-0.815)	0.655 (0.637-0.675)	0.759 (0.724-0.790)	0.406 (0.378-0.440)	0.873 (0.854-0.890)
SUV model	4	0.856 (0.840-0.875)	0.754 (0.739-0.763)	0.736 (0.712-0.751)	0.713 (0.687-0.743)	0.787 (0.759-0.804)
xSPECT model	9	0.932 (0.920-0.944)	0.935 (0.922-0.946)	0.891 (0.870-0.909)	1.000 (1.000-1.000)	0.879 (0.855-0.899)
Combined xSPECT + clinical model	13	0.956 (0.945-0.964)	0.938 (0.925-0.949)	0.880 (0.856-0.899)	1.000 (1.000-1.000)	0.897 (0.876-0.914)